

Effects of Spacer Grid on Thermal-Hydraulic Performance of Fluid in a 4×4 Fuel Channel of VVER-1200 by using Ansys Fluent

MONISHA PODDER PROMA, HUMAYRA ADIBA, AKIFA MUSTAFIZA,
ABDUS SATTAR MOLLAH*

Department of Nuclear Science and Engineering,
Military Institute of Science and Technology,
Dhaka,
BANGLADESH

**Corresponding Author*

Abstract: - In this paper, the structural design of a spacer grid of VVER-1200 has been done by Fusion 360 software. Simulation has been done using Ansys fluent software of temperature profile, velocity profile, and pressure drop along the flow path of fuel assembly to find out the optimum spacing between two spacer grids in a reactor core. Proper spacing between spacer grids helps maintain an optimal coolant, temperature, velocity, and pressure drop ensuring efficient heat removal. This, in turn, contributes to the overall efficiency of the nuclear reactor and generates green energy. The convective heat transfer rate from the fuel rods to the coolant is a crucial factor in determining the total power generation of a nuclear reactor. The resulting impact on heat transfer efficiency directly influences the total power production of the reactor. In general, one of the most important aspects of nuclear power reactor performance is the distribution of temperature, velocity, and pressure along a sub-channel with a spacer grid. To increase heat transfer and turbulent flow, which can raise the reactor's power efficiency, the spacer grid structure is necessary. The distribution of temperature, pressure, and velocity along a sub-channel with a spacer grid is a critical factor that optimizes the circumstances for efficient heat transfer, as may be inferred from the result. The modeling of 4x4 fuel rod assemblies and the prediction of temperature, pressure drop, and velocity distribution along the coolant flow direction have both been accomplished with success using the Ansys Fluent program. Additionally, various PWR-based nuclear power reactor subchannels can use this process.

Key-Words: - spacer grid, optimum spacing, heat transfer, pressure distribution, temperature distribution, Ansys.

Received: April 25, 2024. Revised: October 29, 2024. Accepted: November 17, 2024. Published: December 31, 2024.

1 Introduction

Nuclear power reactors will continue to play a significant part in electricity generation because of their low emission of greenhouse gases, which may be used to mitigate the rising threat of global environmental crises, such as global warming and climate change, which are caused by the consumption of carbon-based fuel, [1], [2], [3]. Additionally, nuclear power generates green energy, which aids in the creation of a society with zero carbon emissions. In the age of climate change, this is one practical application of nuclear energy that differs from all other forms of fossil fuel. To make the most of nuclear power, more energy from the nuclear fuel must be extracted. Optimizing the reactor's internal heat transport is a crucial step in achieving this. A key component of nuclear reactor thermal hydraulics is enhancing heat transport in

sub-channels, [4], [5], [6], [7], [8], [9], [10]. By mixing the flow in sub-channels, spacer grids offer an efficient way to improve turbulent heat transfer [11], [12], [13] and [14].

Spacer frameworks are parts utilized in nuclear reactors to keep a decent separation between fuel rods and to forestall their movement during fluid flow. The essential capability of these frameworks is to guarantee that fuel rods are uniformly separated and isolated by a proper distance. Notwithstanding their essential capability, spacer matrices go about as critical parts in nuclear fuel assemblies, enhancing the circumstances for successful heat move. By limiting problem areas, expanding disturbance and blending, boosting surface region, bringing down vibrations, and advancing uniform coolant stream, spacer frameworks further improve

the heat transfer rate, and ultimately, thermal energy stations' effectiveness.

The numerical study shows [11], [12], [13], [14] that the spacer grid increases the velocity of the fluid near it, which results in fluctuations in the velocity profile. An increase in pressure drop is seen in the places where the spacer grids are positioned. Spacer grids also cause variations in temperature profiles. While the fluid's overall temperature is minimal over the whole channel, it is maximum where spacer grids are positioned. All these features ensure efficient heat transfer and, thus, contribute to the overall efficiency. The goals of high-efficiency power plants are maximum heat extraction from the fuel source and maximum conversion of that heat into electrical power. So, this study intends to demonstrate how the design of the spacer grid structure in a nuclear power plant contributes to producing more electricity while lowering carbon emissions and having a positive impact on climate change, which leads us towards green energy solutions.

In a prior study [4], [5] on VVER-1200 sub-channels, authors used Ansys Fluent to perform thermal hydraulic analysis for various subchannels of the generic VVER-1200 without considering the spacer grid structure. In this study, the structural design of a VVER-1200 spacer grid in a 4-rod subchannel is demonstrated which is used in the Rooppur Nuclear Power Plant (RNPP), Bangladesh.

2 Objectives

Following the above discussion, the objectives of this work have been set as follows:

- To use Ansys Fluent modeling software to create a three-dimensional (3D) model of a spacer grid and the 4x4 fuel rods sub-assembly arrangement in a nuclear power reactor.
- To predict the velocity profile and pressure distribution within the fuel assembly using Ansys Fluent, [5], [10], [15].
- To analyze overall temperature distributions in the model using Ansys Fluent.

3 Methodology

The pressurized water reactor VVER-1200 has 163 fuel components and an open hexagonal core shape. The fuel assembly is made up of 312 fuel rods stacked hexagonally. Thirteen spacer grids were included in the 3750 -mm-long rod bundle design, [16]. A zirconium alloy tube serves as the fuel rod cladding. Particles of sintered UO₂ with the highest enrichment of 5% (4.95±0.05) are arranged inside

the cladding. A fuel rod's average linear heat rate is 167.8 W/cm. The generic layout of the VVER-1200 reactor is shown in Figure 1. There are three different values for the minimum inlet velocity, maximum coolant outlet temperature, and maximum fuel temperature: 5.6 (m/s), 330.96 (°C), and 1345.8 (°C). A typical fuel assembly diagram with four roded sub-channels is shown in Figure 1. The typical fuel assembly with a spacer grid, [16] of VVER-1200 reactor is shown in Figure 2.

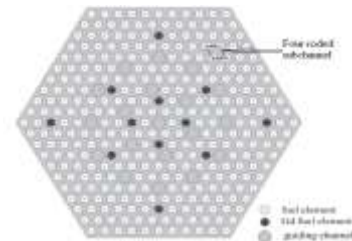


Fig. 1: Typical fuel assembly diagram of VVER-1200. Fuel rods, guide tubes, and four roded sub-channel arrangement

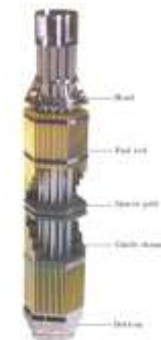


Fig. 2: Typical fuel assembly with spacer grid of VVER-1200 reactor

3.1 Geometry and Coolant Channel

3.1.1 Geometry

Making a geometry is the first and most important stage in any form of analysis. In Fusion360, a basic diagram of the spacer grid and coolant flow path is created. Figure 3(a) is the geometry which is then produced in the same program, followed by modeling. The fuel channel with a spacer grid structure is a major element of a nuclear reactor. The fuel channel is a cylindrical tube containing fuel rods, while the spacer grid helps support and space them properly. The spacer grid consists of metal plates arranged in a grid pattern, with small openings for coolant flow. It should be painstakingly intended to fit the fuel rods and keep up with legitimate dividing, with reasonable openings for the coolant stream. Figure 3(b) shows the 3D model of the liquid area, focusing on the spacer framework view. The spacer grid setup and

coolant flow channel geometry are basic to the proficient and safe activity of an atomic reactor. The dispersing between fuel rods should be painstakingly controlled to guarantee that there is adequate cooling and balance of the nuclear reaction, while likewise keeping the fuel rods from coming into contact with each other which could cause a quick expansion in temperature and possibly lead to a deficiency of coolant or even an implosion.

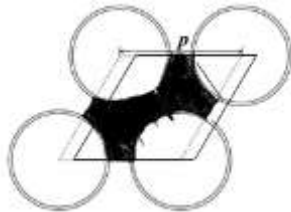


Fig. 3(a): Subchannel containing four nuclear fuel rods. p =pitch of the fuel assembly

Figure 3(b) is the sketch of the outer wall of a sub-channel designed to maximize the flow of heat between the coolant and the fuel rods. The thickness, height, and width of the wall are all important factors affecting the sub-channel's ability to conduct heat and transfer it to the coolant. Overall, the geometry of a fuel channel with a spacer grid is designed to maximize the efficiency and control of the nuclear reaction within the nuclear reactor, while also minimizing the risk of accidents or other problems.



Fig. 3(b): The geometry of the outer wall and spacer grid along with an intent image of the internal view.

For this geometry, the dimensions of the different parts of the model as well as the dimension of the spacer grid are very important which are mentioned in Table 1 and Table 2, respectively.

Heat energy is created in nuclear power plants by nuclear fission reaction in fuel rods and its subsequent transfer to a liquid coolant that circulates in the space between the rods. Nuclear fuel rods arranged in parallel form the rod bundle. The pressure water's hydrodynamics are impacted by the spacer grids. The flow area through the rod bundle is locally decreased by the spacer grids. This results in areas upstream and downstream of the spacer grid

structure experiencing an acceleration and slowing of flow, respectively. We can anticipate and prevent any effects associated with changes in fluid characteristics thanks to the fluid distribution. The lack of sufficient computer hardware makes it challenging to examine the entire rod bundle's flow field. As a result, the first 180 mm of a four-rod bundle with two spacer grids (out of 13 spacer grids) was chosen for examination. Figure 4 shows schematics of the rod and spacer grid computational domain. Figure 5 shows the sketch of the coolant channel along the spacer grid structure. An intent view of the spacer grid structure along with a 3D model of the fluid domain is depicted in Figure 6.

Table 1. Dimensions of the various Ansys model components

Elements	Values of Ansys model (mm)
Height	180
1 st Spacer Grid Location	60
2 nd Spacer Grid Location	120
Fuel Rod Diameter	9.1
Pitch	12.375

Table 2. Spacer grid dimensions

Element	Model Value (mm)
Thickness	2
Length	2
Width	1.29

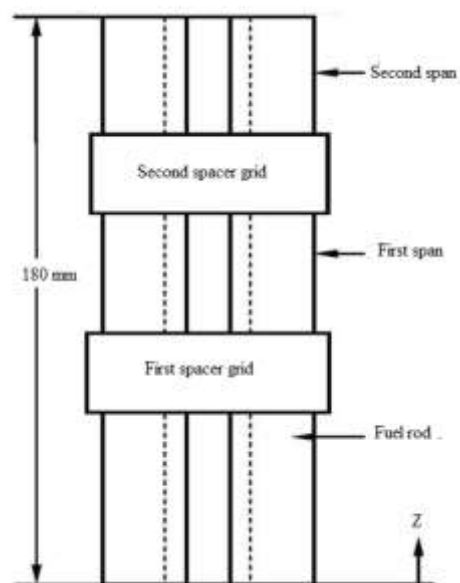


Fig. 4: Computational domain

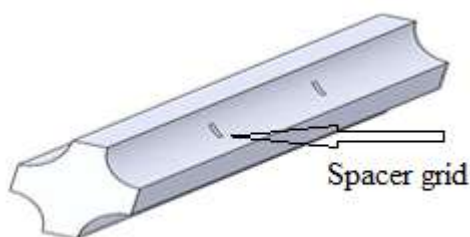


Fig. 5: Diagram of coolant channel along with the spacer grids



Fig. 6: A focused view of the spacer grid along with a 3D model of the fluid domain

The structural integrity of the fuel rods is maintained by a sequence of spacer grids arranged axially along the rod bundle. The spacer grids have an impact on the hydrodynamics of the pressured water and the heat transmission from the fuel rods in addition to their placement. The flow area through the rod bundle is locally decreased by the spacer grids. This results in areas upstream and downstream of the spacer grid experiencing an acceleration and slowing of flow, respectively. A spacer grid prevents the formation of the thermal and hydrodynamic boundary layer along the rod surfaces. Furthermore, the spacer grid intensifies the turbulence in the flow immediately downstream of it.

3.2 Simulation with Ansys fluent

Ansys Fluent is a computational fluid dynamics (CFD) software that uses the finite volume method (FVM) to discretize the governing equations of fluid flow, [17], [18], [19], [20]. Here are a few motivations behind why the FVM is a famous decision in Ansys Fluent and other CFD programming, [15]:

- FVM is a mathematical technique used to mimic liquid stream issues by isolating the liquid space into little control volumes and applying the regulations of protection of energy, force, and mass to each volume.

- FVM monitors mass, force, and energy, and that implies that it can precisely reproduce the conduct of liquids.
- FVM is truly adept at dealing with complex calculations and catching neighborhood varieties in the stream field, which is significant for some engineering applications.
- FVM is numerically steady and computationally proficient, which permits ANSYS fluent to mimic enormous and complex liquid stream issues in a sensible measure of time.
- FVM is an adaptable and dependable strategy for reproducing liquid streams, which is the reason it is broadly utilized in Ansys fluent and other computational fluid dynamics programming.

3.3 Governing Equations

The cooling fluid is incompressible, and the flow is regarded as a steady-state. The computation domain is shown in Figure 1. This domain is made up of four inline-disposed fuel rods. In the cross-section, the cooling fluid is moving against gravity from the bottom to the top of the domain. Each fuel rod's quarter part transfers heat to the cooling fluid. Eqs. (1, 2, and 3) provide the conservation equations [5], [10], [15] for continuity, momentum, and energy at steady state, respectively:

- Continuity:

$$\nabla(\rho \vec{U}) = 0 \quad (1)$$

- Momentum:

$$\nabla(\rho \vec{U} \vec{U}) = -\nabla p + \rho \vec{g} + \nabla[\mu(\nabla \vec{U} + (\nabla \vec{U})^T)] \quad (2)$$

- Energy

$$\nabla[(\rho E + p)\vec{U}] = \nabla[(k\nabla T) - \sum_j h_j \vec{j}_j + (\vec{\tau} \cdot \vec{U})] + S \quad (3)$$

where ρ is the fluid density, \vec{U} the velocity vector of fluid, p is the pressure, μ is the shear viscosity of fluid, \vec{g} is the gravity vector, k is the thermal conductivity, E is the total energy, $\vec{\tau}$ is the viscous stress tensor, S is the source term, h_j is the convective heat transfer coefficient, \vec{j}_j is the velocity of each species and T is the fluid temperature at the entry of the channel.

The continuity equation (1) represents the conservation of mass in fluid dynamics. It states that for any given control volume, the mass entering the volume must equal the mass leaving it, ensuring no mass is lost or gained within the volume. It ensures the conservation of the fluid's mass, which means

that the fluid's density and velocity must change throughout motion to preserve this conservation.

The momentum equation (2) is acquired by executing Newton's second law to smooth fluid movement. The term $\rho \vec{u} \vec{u}$ addresses the convective transport of momentum. ∇p represents the force coming from fluid pressure gradients. $\rho \vec{g}$ demonstrates the gravitational force working on the fluid. The term $\mu (\nabla \vec{u})^T$ represents the liquid's viscous forces, where μ is the dynamic viscosity, and $\nabla \vec{u}$ is the velocity gradient tensor. This condition decides how the liquid advances under the effect of several forces, like gravity, pressure inclinations, and viscous stresses. Set all the more forth plainly, it portrays how the liquid's momentum changes in light of the external and internal forces following up on it.

The liquid's energy preservation is represented by the energy equation (3). The total energy per unit volume is signified by the image ρE , where E incorporates both internal energy and kinetic energy, p is the pressure, and $p \vec{u}$ demonstrates the work done by pressure forces. The liquid's heat conduction is addressed by $k \nabla T$, where T is the temperature and k is the thermal conductivity. The aggregate $\sum_j h_j \vec{j}_j$ shows the transmission of energy coming about because of mass dispersion, where h_j is the particular enthalpy of species j , and \vec{j}_j is the dispersion motion of species j . $\vec{\tau} \cdot \vec{u}$ addresses any extra energy contributions, for example, viscous dispersal and S addresses any outer sources or sinks of energy. This condition makes sense of the conveyance and preservation of liquid energy while thinking about heat conduction, pressure work, and outside energy sources also, sinks into account. It integrates the effects of mechanical energy (work done by forces), nuclear power (heat), and other energy trades happening inside the liquid.

3.4 Mesh Generation and Analysis

3.4.1 Material Selection

The choice of materials is a basic move toward designing examination as it straightforwardly impacts the execution and toughness of the end result. The selection of material is guided by its chemical and physical properties, which vary depending on the specific analysis requirements. Table 3 and Table 4 summarize the key chemical and physical properties of mild steel, a material often chosen for its balanced combination of strength, ductility, and machinability.

Table 3. Chemical properties of mild steel

Material	Percentage
C	0.17 %
Mn	0.54 %
P	0.16 %
Fe	98.7 %
Si	0.20 %

Table 4. Physical properties of mild steel (white)

Property	Value
Heat Capacity	510 J/g K
Melting Point	1450 °C
Thermal Conductivity	50 W/(m. K)
Thermal Expansion	11.8 to 12.2 $\mu\text{m}/(\text{m. K})$

The chemical composition of mild steel significantly impacts its mechanical properties, such as strength, hardness, and corrosion resistance. Table 3 outlines the typical chemical composition of mild steel. The physical properties of mild steel, such as heat capacity, melting point, thermal conductivity, and thermal expansion, determine how the material responds to thermal loads and mechanical stresses.

3.4.2 Mesh Generation

Mesh generation, [15], [21], [22], [23], [24], involves dividing a continuous geometric space into discrete geometric and topological cells to create a mesh size. A mesh network is created when these cells and points come together (Figure 7). It can be nearly any size or shape and is used to solve partial differential equations. Each of the mesh's cells represents a different approach to solving the issue, which when combined across the entire network results in a mesh-wide solution. Figure 8 showing a mesh of the solution. The mesh is generated by using Ansys fluent workbench, [15].

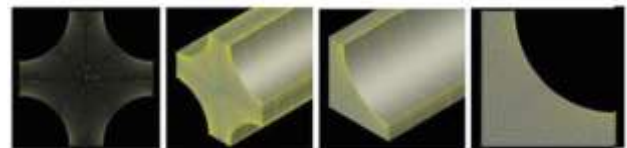


Fig. 7: Channel meshing

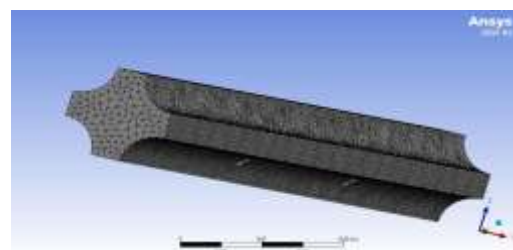


Fig. 8: Mesh of the flow domain using a spacer grid

3.4.3 Mesh Sensitivity Analysis

Mesh independence test for outlet temperature is shown in Figure 9. The outlet temperature for mesh size >2 millions is almost stable which indicates the independence of mesh size.

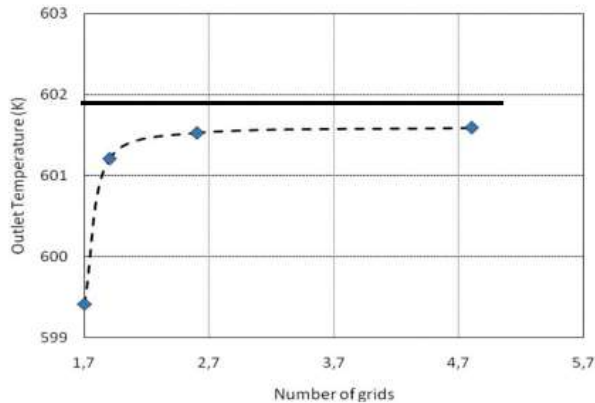


Fig. 9: Mesh independence test at hot leg locations for various grid cell counts; the black solid line is the VVER-1200's design value for the outlet temperature

Mesh sensitivity analysis is a crucial aspect of the mesh generation process. It involves systematically refining the mesh and evaluating how the changes impact the solution. The purpose of mesh sensitivity analysis is to guarantee that the outcomes are unaffected by the mesh size so that additional refinement would not substantially change the solution. This is vital for validating the simulation's precision and dependability.

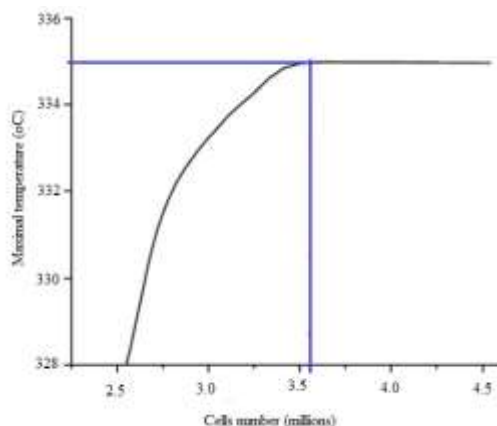


Fig. 10: Mesh sensitivity

Reducing the number of mesh cells without compromising the accuracy and dependability of the output is the goal of mesh sensitivity. To put it another way, to ensure that the outcomes are independent of the mesh that was utilized. Ten meshes were tested in order to confirm this condition. For the ten meshes, the profile of the

maximum temperature is depicted near the channel's departure. There were between 2.7 and 4.5 million cells. The mesh selection is the one where the temperature profile remains constant. Figure 10 displays the results that were achieved. The mesh that will be utilized in this investigation is the one with 3.6 million cells since it is the one where the maximum temperature remains constant.

1) Importance of Mesh Sensitivity:

a) Accuracy: A mesh that is too coarse may fail to capture essential physical phenomena, leading to inaccurate results. On the other hand, a finely refined mesh can work on precision by better addressing complex calculations and slopes.

b) Computational Cost: Mesh sensitivity examination assists in deciding the ideal cross-section with estimating that offsets precision with computational effectiveness. It forestalls superfluous refinement that could increment computational time and asset use.

2) Procedure for Mesh Sensitivity Analysis:

a) Initial Mesh: Begin with an underlying mesh based on the calculation and anticipated arrangement conduct. This mesh ought to be adequately coarse to take into account fast calculation yet fine to the point of catching basic elements.

b) Refinement: Step by step refine the mesh in districts where higher slopes or massive changes in arrangement factors are normal. This could include diminishing the element size or expanding the number of elements in those areas.

c) Convergence Study: Play out an intermingling concentrate by contrasting outcomes and different mesh densities. The arrangement ought to join to a steady value as the mesh is refined. Assuming huge changes are noticed, further refinement is vital.

d) Validation: Approve the final mesh by contrasting the recreation results and trial information or then again logical arrangements, if accessible. That's why this step guarantees the mesh is adequately refined to give precise outcomes.

By leading cross-section awareness investigations, engineers can guarantee that the simulation results are strong and dependable, giving trust in the plan and analysis process, [15].

The goal is to create a mesh with high-quality (well-shaped) cells that accurately depict the geometry of the input domain without having too many cells to prevent additional computations. Furthermore, the model's mesh must be fine (have tiny components) in areas that are essential for the calculations that follow, [24]. The fine meshing in

Figure 11 shows that the geometry is robust and appropriate for the design.

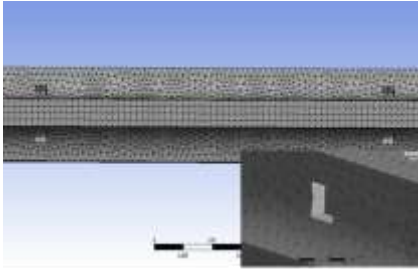


Fig. 11: Mesh of different positions of the full fluid domain with a focused view of the spacer grid structure

Moreover, the mesh works with the utilization of mathematical strategies, for example, FEM or FVM to settle the governing conditions. Also, it allows the application of different limit conditions and loads expected in mimicking certifiable actual peculiarities. The nature of the mesh is pivotal, as a very much-planned mesh guarantees the steadiness, precision, and dependability of the simulation results, [25].

Table 5 in this context contains the statistics for the experiment's mesh. In Ansys, a node is a point in space where values of solution variables like temperature, pressure, and velocity are stored. These nodes are used to divide a complex geometry into smaller, simpler elements for solving complex problems. Nodes are connected by edges to form a mesh that covers the entire domain of interest. The solution variables at each node are used to compute the solution for the entire model, providing a detailed representation of the physical behavior of the system. The accuracy and reliability of Ansys simulations depend on the number and distribution of nodes used in the mesh. The sizing of mesh components and the number of elements and nodes created due to meshing are listed in Table 5.

Table 5. Mesh statistics

Parameters	Defined by	Remarks
Mesh Method	Body Sizing	Per Element Size: 100 mm
Mesh Statistics	Nodes	379863
	Elements	159692
Physics Preference	Mechanical	-

3.4.4 Boundary Conditions

For a boundary value problem to be resolved, boundary criteria must be met. The external forces acting on the part or the body force as a result of the component's weight are defined. The boundary conditions for the experiment are given in Table 6.

Table 6. Boundary condition

Inlet boundary pressure	16.1 MPa
Inlet temperature	571.5 K
Inlet velocity	5.67 m/s
Heat flux	278000 W/m ²
Volumetric mass flow	4000 kg/m ³

3.4.5 Solution Procedure in Ansys Fluent

Ansys Fluent uses the phase-coupled SIMPLE (PC-SIMPLE) method for the pressure-velocity coupling, [15]. The basic steps in the Ansys Fluent CFD study are:

1. Establishing geometry.
2. Physical configuration.
3. Generation of meshes.
4. Setup of the solution.
5. Solver run.
6. Initialization.
7. Post-processing.
8. Evaluation and analysis.

The flow chart for the solution procedure is given [15] in Figure 12:

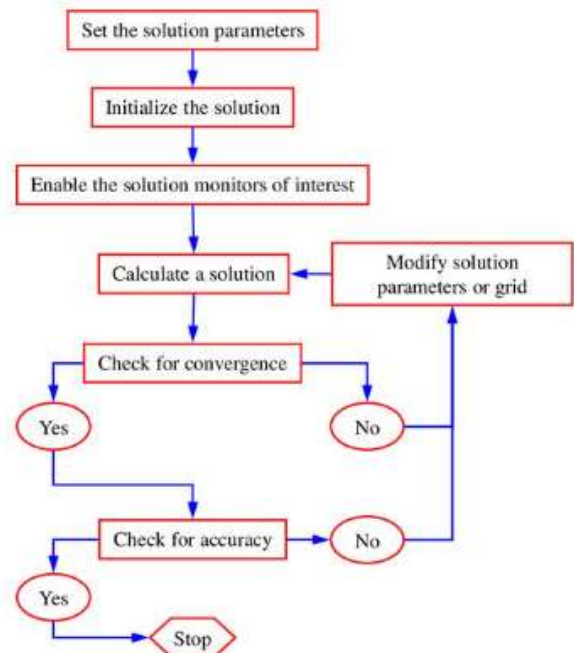


Fig. 12: Flow chart for the solution procedure

The distinction between the governing equations' exact solutions and the numerical solution produced by the solver is referred to as the "residual" in Ansys Fluent. The residual is used to assess whether or not the solution has converged. It serves as a gauge for the numerical solution's accuracy. By continuously updating the solution until the residual falls below a pre-set tolerance threshold, the solver makes an effort to minimize the residual during the solution process. The residual is commonly expressed using the norm of the residual vector, which is a vector that contains the residuals for each equation being solved. There are many kinds of residuals in Ansys Fluent depending on the type of problem being solved. For example, in the momentum equation for fluid flow, the residual vector comprises the pressure residuals and the velocity's x, y, and z components. Monitoring the residual throughout the solution process is essential to ensure that the solution has converged to a reasonable degree of precision. To get a better solution, it could be essential to change the mesh or the solver settings if the residual does not converge.

For a generic variable ϕ at cell P, the conservation equation can be expressed as follows after discretization:

$$a_P \phi_P = \sum_{nb} a_{nb} \phi_{nb} + b \quad (4)$$

The center coefficient, in this case, is a_P , the influence coefficients for the surrounding cells are a_{nb} , and the boundary conditions and constant part of the source term S_c in $S = S_c + S_P \phi$ are represented by b . Equation 4 states:

$$a_P = \sum_{nb} a_{nb} - S_P \quad (5)$$

The imbalance in Equation (4) is the residual R^ϕ , which is calculated by the pressure-based solver of Ansys Fluent. This value is then totaled over all computational cells P. We call this residual the "unscaled" residual, expressed as:

$$R^\phi = \sum_{\text{cells } P} \left| \sum_{nb} a_{nb} \phi_{nb} + b - a_P \phi_P \right| \quad (6)$$

Ansys Fluent employs a scaling factor that is indicative of the ϕ flow rate across the domain to scale the residual. The definition of this "scaled" residual is:

$$R^\phi = \frac{\sum_{\text{cells } P} \left| \sum_{nb} a_{nb} \phi_{nb} + b - a_P \phi_P \right|}{\sum_{\text{cells } P} |a_P \phi_P|} \quad (7)$$

There aren't any common metrics to assess convergence. When applied to other kinds of problems, residual definitions that work well for one class of problems may be deceptive. Thus, it is a good idea to monitor pertinent integrated parameters like drag or heat transfer coefficient in addition to looking at residual levels while judging convergence. The Ansys Fluent default convergence criterion is adequate for the majority of cases [15]. This criterion states that for all equations-with the exception of the energy, for which the criterion is 10^{-6} -the scaled residuals must decline to 10^{-3} . The residuals must, as stated, decrease to 10^{-3} . This indicates that the residual should eventually drop to 10^{-3} (Figure 13), regardless of where it begins.

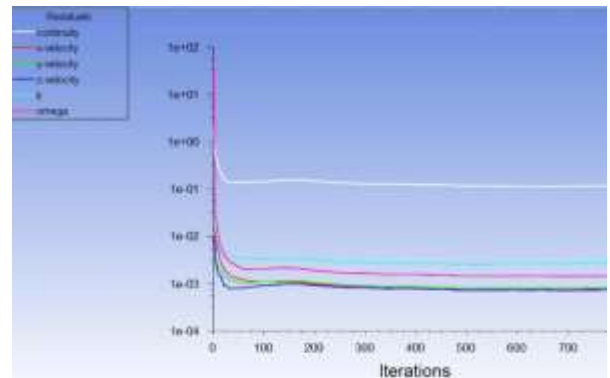


Fig. 13: Convergence and residual

4 Uncertainties and Errors

Remember that numerical solutions are only approximations when working with problems involving fluid flows and heat transfer. Three types of systematic mistakes are invariably present in the numerical solutions: modeling errors, discretization errors, and iteration faults. The hardest mistakes to estimate in modeling are those that require highly accurate experimental data, or at the very least, data from a few test cases with precise and comprehensive results. Once the discretization and iteration errors are computed, the modeling mistakes are examined. When there is a discrepancy between the exact solutions of the modeling equations and the algebraic system that results from discretizing these equations, mistakes such as discretization errors occur, [25]. An ideal grid should be as densely packed and orthogonal as feasible in areas where significant truncation errors are anticipated.

The discrepancy between the exact and iterative solutions of the system of algebraic equations is known as the iteration errors, [25], [26]. Knowing when to end an iteration is crucial when performing any type of simulation. Iteration errors should, as a starting point, be at least an order of magnitude

smaller than discretization errors. The rate at which the residuals decrease can be used to examine the pace of error reduction because it is closely related to the rate at which the differences between two subsequent iterations are reduced, with the exception of the first iteration. This means that if the residual norm has decreased by 3–4 orders of magnitude and one knows the error level at the beginning of the computation, the error will undoubtedly decline by 2-3 orders of magnitude. Thus, the solution is correct within the range of 0.1 to 1.5% since the first two or three most significant numbers won't change in subsequent iterations, [26].

5 Results and Discussions

5.1 Outcomes of the Numerical Simulation

Steel material is considered as the structural material for the simulation. Proper mesh is generated, and the boundary conditions are applied. The Ansys solver generates a solution according to the boundary condition and the parameters being investigated for the work i.e. pressure, velocity, and temperature.

5.2 Velocity Profile

Figure 14 is the distribution of velocity which is easily understood from the contour plot that is displayed after completion of the solution, where red color indicates maximum velocity and blue color indicates minimum velocity. Also, the range of the velocity is displayed in the software. The internal velocity is varied from 5.65 m/s to 6.9 m/s. Figure 13 shows the velocity distribution from 5.65 m/s to 6.9 m/s of the spacer grid-designed simulated sub-channel. As there is no obstacle, it demonstrates that the fluid is flowing at the highest velocity in the center of the sub-channel, highlighted by a red contour. However, the velocity towards the wall is zero, highlighted by a blue contour.

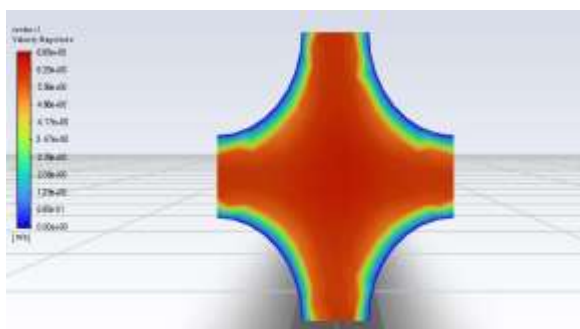


Fig. 14: Velocity distribution of the sub-channel with spacer grid design

The reason for these zero velocities is the fluid's friction against the wall. It occurs due to the drag force developed in the fluid flow because of contact with the wall surface. Figure 15 shows a blue contour color which suggests that there is no velocity present on the wall side.



Fig. 15: Velocity distribution of wall

Figure 16 shows the variation of velocity of the coolant as it flows through the sub-channel along with the axial direction. The presence of spacer grids can cause an increase in velocity near the spacer grid due to the factors listed below:

(i) *Flow acceleration*: The spacer grid creates obstructions to the coolant flow, which can cause the coolant to accelerate as it traverses the openings between the spacer grid structure and the nuclear fuel rods. This flow speed increase can bring about an expansion in velocity in the district close to the spacer grid.

(ii) *Flow constriction*: The spacer framework makes thin gaps between the fuel rods, which can result in choking of the coolant stream. This choking can cause an expansion in velocity in the district close to the spacer grid.

(iii) *Flow separation*: The spacer framework can cause the coolant stream to be isolated from the nuclear fuel elements and reattached downstream of the spacer grid structure. This reattachment can bring about a vortex or distribution zone, which can cause an expansion in velocity in the area vicinity of the spacer grid elements, [10]. This reattachment can bring about a vortex or distribution zone, which can cause an expansion in velocity in the area near the spacer grid structure. The graph typically shows the maximum velocity occurs at the position before colliding with the second spacer grid at 120 mm from the bottom and immediately it decreases after the collision.

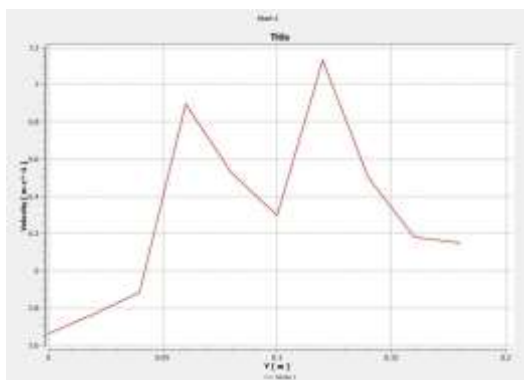


Fig. 16: Velocity vs position graph of a spacer grid

In fluid dynamics, when an obstruction (such as a baffle) is introduced in a pipe, the fluid flow velocity increases as it gets through the narrow openings around the obstruction, similar to the flow constriction caused by the spacer grid in this study. This phenomenon is well-documented in studies of pipe flow, where velocity profiles are measured before and after obstructions, [11].

Experimental studies on pipe flow with obstructions show a marked increase in velocity at the constriction points, which matches the velocity increase observed near the spacer grid in this analysis. The velocity trends seen in the sub-channel are thus validated. Heat exchanger tubes are supported by spacer grids, which produce flow constrictions that raise velocities at particular locations inside the exchanger. The impact of the spacer grid in this investigation is seen in this. This observation is consistent with CFD simulations of heat exchangers, which frequently show higher velocities close to the spacers. Both CFD calculations and experimental observations confirm the rise in velocity in heat exchangers close to spacer grids, showing a strong parallel to the velocity fluctuations in the sub-channel with a spacer grid. These illustrations show how the velocity profile found in this investigation aligns with accepted fluid dynamics concepts. The validation ensures that the findings of this study are accurate and representative of real-world fluid behavior.

5.3 Pressure Distribution

The distribution of pressure is easily understood from the contour plot that is displayed after completion of the solution, where red color indicates maximum pressure and blue color indicates minimum pressure. Also, the range of the pressure is displayed in the software. The internal pressure is varied throughout the whole distance. Figure 17 shows the pressure distribution of the spacer grid-designed simulated subchannel.

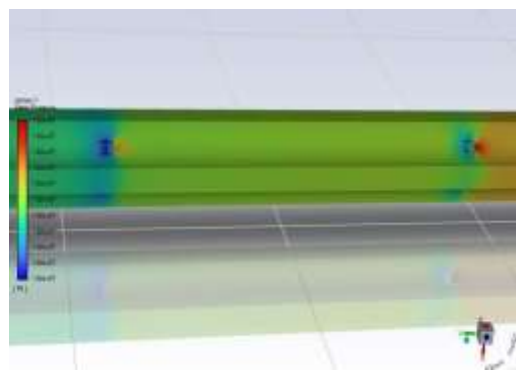


Fig. 17: Pressure distribution of the sub-channel with spacer grid design

At the locations of the spacer grids, it can be observed that the pressure is reduced to almost a minimum. The pressure decrease in the spacer grid area can be observed through the blue contour. While constructing and managing nuclear fuel assemblies, the pressure drop near the spacer grid is a critical aspect to be considered. Figure 18 demonstrates the pressure distribution of the outer wall which is influenced by various factors.

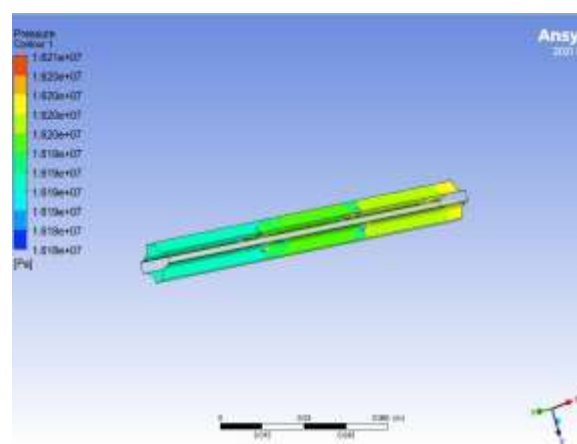


Fig. 18: Pressure distribution of outer wall

Those factors are the flow of coolant through the reactor, the design and materials of the fuel rod, and the pressure inside the reactor vessel. For the fuel rod to remain structurally stable and not collapse or distort, the pressure on its outside wall is essential. The coolant's flow pressure change as it gets through the subchannel is depicted in Figure 19. These spacer grids have the potential to increase the coolant flow's pressure drop. There are several reasons for this pressure reduction, including:

- (i) Flow resistance: The coolant flow is obstructed by the spacer grids, increasing flow resistance and resulting in a pressure drop.

- (ii) Turbulence: The coolant flow may become turbulent due to the spacer grids, which raises the pressure drop and flow resistance even more.
- (iii) Vibration: The flow-induced forces may cause the spacer grids to vibrate, which may result in an additional drop in coolant flow pressure.
- (iv) Mixing: The coolant flow may be mixed by the spacer grids, which may result in a pressure drop because of variations in flow velocity and direction.

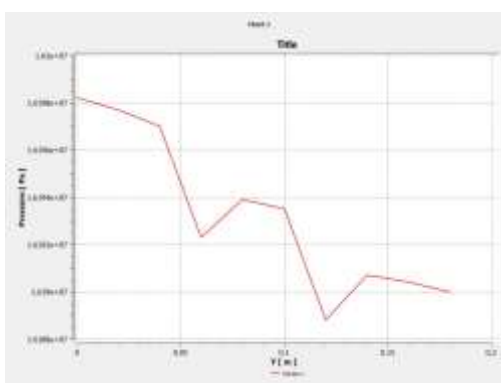


Fig. 19: Pressure vs position graph of a spacer grid

The vertical axis shows the fluid pressure at that point, while the horizontal axis shows the position along the subchannel. The graph typically shows the lowest pressure at the point 120 mm from the bottom, right before impact with the second spacer grid, and the pressure immediately rises after hit. The spacer grid, a device placed inside the subchannel to guarantee the correct spacing between fuel rods, might change the velocity profile due to its impact on the flow pattern. Consequently, the graph can provide valuable information on the design and optimization of nuclear fuel assemblies. Pressure declines happen when fluid passes through a conduit with bends because of the direction change and higher frictional resistance. This scenario is similar to the pressure drop induced by spacer grids, where the flow direction changes and resistance increases. Theoretical models, such as the Bernoulli equation adjusted for losses, and experimental measurements consistently show that pressure drops in pipe bends correlate with the degree of the bend and the flow velocity, validating the pressure behavior observed in the sub-channel.

In heat exchangers, baffles are used to direct the flow and enhance heat transfer, but they also cause significant pressure drops. This is similar to the effect of spacer grids in this study, where flow obstructions lead to pressure reductions. FD simulations and experimental studies of heat exchangers with baffles show a clear correlation between baffle placement and pressure drop. These findings align with the pressure distribution patterns

observed near spacer grids, reinforcing the validity of the results.

5.4 Temperature Profile

The distribution of temperature is easily understood from the contour plot that is displayed after completion of the solution, where maximum temperature is indicated by red color and minimum temperature is indicated by blue color. Also, the range of the temperature is displayed in the software. The internal temperature varies from 571.2 K to 571.56 K. Figure 20 demonstrates that the temperature of the sub-channel is minimum at the bottom, as shown by the blue contour, and gradually rises towards the top.

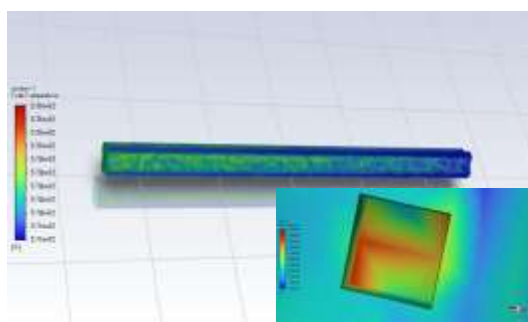


Fig. 20: Sub-channel temperature distribution using a spacer grid design

The temperature is at its highest where the spacer grids are located. It is visible in the focused image of the spacer grid region and is denoted by the contour that is colored in red. Figure 21 indicates the temperature distribution of the outer wall of a fuel rod typically increases from the bottom to the top of the rod, reflecting the increasing heat generation of the nuclear fuel as it undergoes fission.

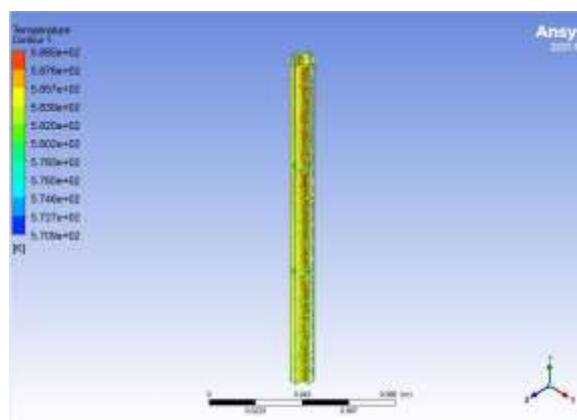


Fig. 21: Temperature distribution of the outer wall

The highest temperature is typically found near the top of the fuel rod, where the fission reactions

are most intense. The temperature distribution along the length of the fuel rod is also affected by the flow of coolant through the reactor. Coolant flowing around the fuel rod absorbs heat from the outer surface of the rod and carries it away, helping to regulate the temperature and prevent overheating. The flow of coolant is carefully designed to maintain a consistent temperature distribution and prevent hot spots from developing. The temperature vs. location graph of a spacer grid in Figure 22 illustrates how the fluid's temperature changes as it passes through the subchannel. The vertical axis shows the temperature of the fluid at that point, while the horizontal axis shows the position along the subchannel. The graph typically shows that the temperature increases with the distance of the subchannel.

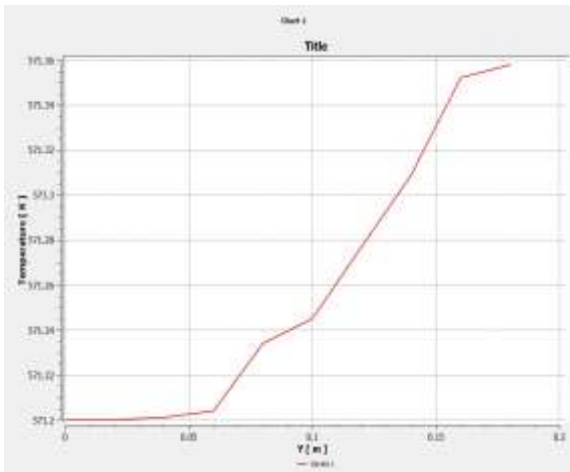


Fig. 22: A spacer grid's temperature vs. location graph illustrates the temperature variation

Because of its effect on the flow pattern, the spacer grid—a device positioned inside the sub-channel to ensure the proper spacing between fuel rods—can alter the velocity profile. As a result, the graph can offer useful information on nuclear fuel assembly design and optimization. Two factors that influence temperature distribution are the heat generated by the fuel rods and the heat transfer between the rods and the coolant. Spacer grids can improve heat transmission and promote turbulent flow, resulting in a more even temperature distribution. Another important factor that may affect reactor performance is velocity distribution. Spacer grids can promote turbulent flow and improve velocity distribution, which can enhance heat transfer.

The pressure distribution in sub-channels is influenced by the coolant flow rate and spacer grid geometry. The spacer grid can cause a pressure drop, which can affect reactor performance.

For complex flows with complex geometry, CFD simulations need to do a grid sensitivity analysis. However, there are instances where it is limited by useful factors like computing power. In order to undertake a thorough grid independence investigation, grid systems of roughly 1.7 million, 1.9 million, 2.6 million, and 4.8 million meshes are used, respectively, for the current CFD analyses. It confirms that results for output temperature are not significantly affected by refined meshes larger than 4.8 million. For the remaining investigations, 4.8 million meshes are chosen in consideration of computational time and capability.

6 Conclusions

From the result, we can conclude that the distribution of temperature, velocity, and pressure along a sub-channel with a spacer grid is a crucial aspect that optimizes the conditions for effective heat transfer. A spacer grid is installed in the 4x4 fuel sub-assembly of a PWR-based VVER-1200 to provide support and maintain the proper spacing between the fuel rods, promoting heat transfer between the rods and the coolant. Overall, temperature, velocity, and pressure distribution along a sub-channel with a spacer grid structure is a crucial aspect of nuclear reactor performance. The spacer grid is essential for promoting turbulent flow and enhancing heat transfer, which can improve the reactor's power efficiency.

Future work will focus on developing the full assembly model with 13 spacer grids of the nuclear reactor VVER-1200 in order to enhance the geometric details and conduct a more thorough analysis. The temperature and pressure that are obtained from these simulations can be used as the boundary conditions of a system code to determine the pressure and temperature distributions throughout the assembly's sub-channels in the event of an accident.

Acknowledgment:

The authors would like to give thanks to the Nuclear Modeling and Simulation Laboratory along with associated personalities under the Department of Nuclear Science and Engineering at the Military Institute of Science and Technology.

Declaration of Generative AI and AI-assisted Technologies in the Writing Process

During the preparation of this work the authors used Grammarly for language editing. After using this service, the authors reviewed and edited the content as needed and take full responsibility for the content of the publication.

References:

- [1] Toth FL, Rogner HH (2006) Oil and nuclear: Past, present and future. *Energy Econ.*, 28:1–25.
- [2] Nico Bauer, Robert J. Brecha and Gunnar Luderer (2012). Economics of nuclear power and climate change mitigation policies, *PNAS*, Vol. 109, no. 42, 16805–16810. <http://dx.doi.org/10.1073/pnas.1201264109>.
- [3] A. S. Mollah, Sabiha Sattar, M. A. Hossain, A.Z.M. Salahuddin and H. AR-Rashid (2015). Prospects of Nuclear Energy for Sustainable Energy Development in Bangladesh, *International Journal of Nuclear Energy Science and Engineering (IJNESE)* Vol. 5, 28. doi: 10.14355/ijnese.2015.05.004.
- [4] Taosif Alam and M. A. R. Sarkar (2018). Thermal hydraulics simulation of fuel sub-assembly for 1200 MWe nuclear power reactor, *Proc. of the International Conference on Mechanical, Industrial and Energy Engineering*, 2018, 23-24 December, Khulna, Bangladesh.
- [5] Mosaddak Ahamed Zahid, Md. Imam Mehedi, Shamsul Arefin Shibly A. S. Mollah (2024), Thermal Hydraulic Analysis for Different Subchannels of Generic Thermal Hydraulic Analysis for Different Subchannels of Generic VVER-1200, *International Journal of Nuclear Security*, Vol. 9: No. 2, Article 8. <https://doi.org/10.7290/ijns09147839>.
- [6] Shojaa Ayed Aljassar, Oleg.Yu Dolmatov, Muhammad Saqib and Yubin Xu (2020), Analysis of the coolant flow in sub channels of the VVER-1000 reactor by CFD method, *International Journal of Mechanical and Production Engineering Research and Development (IJMPERD)*, Vol. 10, Issue 2, 1419–1428.
- [7] Lin, C.-H.; Yen, C.-H.; Ferng, Y.-M. (2014). CFD Investigating the Flow Characteristics in a Triangular-Pitch Rod Bundle Using Reynolds Stress Turbulence Model. *Annals of Nuclear Energy*, Vol. 65, 357–364. DOI: 10.1016/j.anucene.2013.11.023.
- [8] H. Ganjiani and B. Firoozabadi (2010). Three dimensional simulation of turbulent flow in 3 sub-channels of a VVER-1000 Reactor, *Transaction B: Mechanical Engineering*, Vol. 17, No. 2, 83-92.
- [9] B. Liu, S. He, C. Moulinec and J. Uribe (2017). Sub-channel CFD for nuclear fuel bundles, *Nuclear Engineering and Design*, Vol. 355, 2019. <http://dx.doi.org/10.1016/j.nucengdes.2019.11.0318>.
- [10] S. K. Vermaa, S. L. Sinhaa, and D. K. Chandrakerb, A Comprehensive Review of the Spacer Effect on Performance of Nuclear Fuel Bundle using Computational Fluid Dynamics Methodology, *Materials Today: Proceedings*, 4 (2017) 10030–10034.
- [11] Moysés A. Navarro1 and André A. C. Santos, Numerical evaluation of flow through a 5x5 pwr rod bundle: effect of the vane arrangement in a spacer grid, *2009 International Nuclear Atlantic Conference - INAC 2009*, Rio de Janeiro, RJ, Brazil, September 27-October 2, 2009 Associação Brasileira De Energia Nuclear - Aben, ISBN: 978-85-99141-03-8.
- [12] Yao, S. C., Hochreiter, L. E., and Leech, W. J. (1982). Heat transfer augmentation in rod bundles near grid spacers”, *Journal of Heat Transfer*, Vol. 104, 76-81. <https://doi.org/10.1115/1.3245071>.
- [13] Chun, T. H., Oh, D. S. (1998). A pressure drop model for spacer grids with and without flow mixing vanes”, *Journal of Nuclear Science and Technology*, Vol. 35, 508-510. <https://doi.org/10.1080/18811248.1998.9733899>.
- [14] Kim, K. Y., and Seo, J. W. (2005), Numerical optimization for the design of a spacer grid with mixing vanes in a pressurized water reactor fuel assembly, *Nuclear Technology*, Vol. 149, 62-70. <https://doi.org/10.13182/NT05-A3579>.
- [15] Basics of CFD Simulation with Ansys Fluent. ANSYS, [Online]. <https://www.ansys.com/academic/educators/education-resources/basics-of-cfd-simulation-with-ansys-fluent> (Accessed Date: November 22, 2024).
- [16] IAEA Status report 107-VVER-1200 (V-392M), [Online]. <https://www.rosatom.ru/upload/iblock/0be/0be1220af25741375138ecd1afb18743.pdf> (Accessed Date: December 14, 2024).

- [17] H.K. Versteeg and T. J. Hughes, An Introduction to Computational Fluid Dynamics: The Finite Volume Method", (2012). The finite element method: linear static and dynamic finite element analysis, New York: Dover Publications.
- [18] M. Mounnassi, Salim Belouettar, Éric Bédet, Stéphane P.A. Bordas, Didier Quoirin, and Michel Potier-Ferry (2011), Finite element analysis on implicitly defined domains: An accurate representation based on arbitrary parametric surfaces, *Computer Methods in Applied Mechanics and Engineering*, Vol. 200, No. 5-8, 774-796. <https://doi.org/10.1016/j.cma.2010.10.002>.
- [19] Munson, B. R., Young, D. F., and Okiishi, T. H. (2009). *Fundamentals of Fluid Mechanics* (6th ed.). Wiley.
- [20] Versteeg, H.K. and Malalasekera, W. (2007). An Introduction to Computational Fluid Dynamics: The Finite Volume Method (2nd Edition), Pearson Education Limited, Harlow, England.
- [21] Chauhan, S and Pankaj Chandna, P. (2017), Experimental investigation on effect of heat treatment on mechanical properties of Steels and Titanium, *International Journal of Current Engineering and Technology*, Vol.7, No.3, 845-850, [Online]. <http://inpressco.com/category/ijcet> (Accessed Date: December 24, 2024).
- [22] Begüm Kütük and Ibrahim Halil Güzelbey (2020). Computational fluid dynamics analyses of a VVER-1200 nuclear reactor vessel for symmetric inlet, asymmetric inlet, and LOCA conditions, *International Journal of Pressure Vessels and Piping* 187 (2020), <https://doi.org/10.1016/j.ijpvp.2020.104165>.
- [23] C. F. M. Schettino (2017), Evaluation of spacer grid spring characteristics by means of physical tests and numerical simulation, 2017 *International Nuclear Atlantic Conference - INAC 2017* Belo Horizonte, MG, Brazil, October 22-27.
- [24] Arun Kumar Singh, Ravi Kant Gupta, Mukesh Kumar, and Kaushalendra Yadav (2023), Review of finite element mesh generation methods, *AIP Conf. Proc.* 2782, 020095, <https://doi.org/10.1063/5.0154340>.
- [25] Roache, P.J., Quantification of uncertainty in computational fluid dynamics, *Annu. Rev. Fluid. Mech.*, Vol. 29, 123-160, 1997. <https://doi.org/10.1146/annurev.fluid.29.1.123>
- [26] Ferziger, J.H, Perić, M., *Computational Methods for Fluid Dynamics*, Springer Verlag, New York, 3rd ed, 2002.

Contribution of Individual Authors to the Creation of a Scientific Article (Ghostwriting Policy)

MPP, HA, and AM performed the analysis, and the simulations and wrote the paper. ASM contributed towards the problem selection, proofread the paper several times, provided guidance throughout the whole preparation of the manuscript, critically revised the paper, and made significant revisions. The final manuscript was read and approved by all authors.

Sources of Funding for Research Presented in a Scientific Article or Scientific Article Itself

No funding was received for conducting this study.

Conflict of Interest

The writers say they have no competing interests.

Creative Commons Attribution License 4.0 (Attribution 4.0 International, CC BY 4.0)

This article is published under the terms of the Creative Commons Attribution License 4.0 https://creativecommons.org/licenses/by/4.0/deed.en_US